Electronic Supplemental Information

Making Light Work: Designing plasmonic structures for the selective photothermal methanation of carbon dioxide

Yi Fen Zhu[a] , Bingqiao Xie[a], Jodie A. Yuwono[a, c], Priyank Kumar[a], Abhinav S. Sharma[b], Michael P. Nielsen[b], Avi Bendavid[d], Rose Amal[a], Jason Scott*[a], Emma C. Lovell*[a]

[a] *Particles and Catalysis Research Group, School of Chemical Engineering, University of New South Wales, NSW 2052, Australia*

[b] *School of Photovoltaic and Renewable Energy Engineering, The University of New South Wales, Sydney, NSW 2052, Australia*

[c] *School of Chemical Engineering and Advanced Materials, The University of Adelaide, Adelaide SA 5005, Australia*

[d] *CSIRO Manufacturing, Lindfield, NSW 2070, Australia*

*jason.scott@unsw.edu.au; *e.lovell@unsw.edu.au

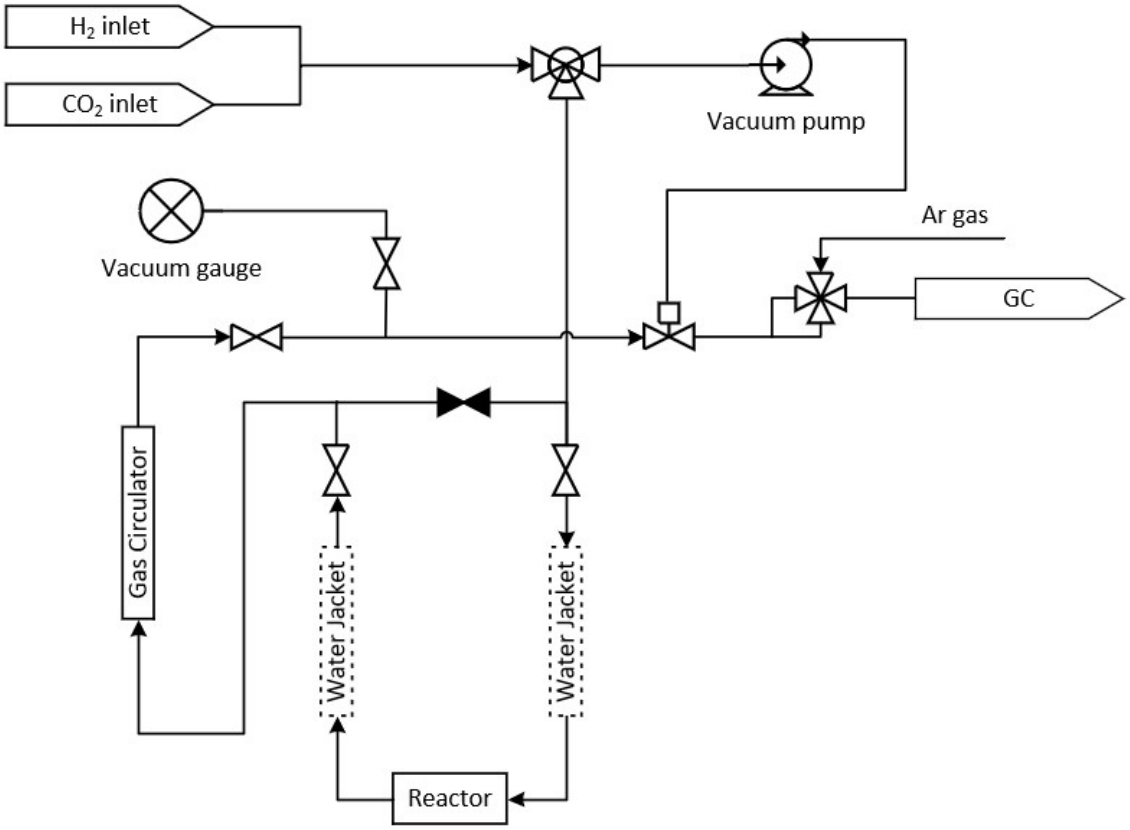

Figure S1.Schematic of batch mode photothermal reactor system used for CO_2 methanation reaction.

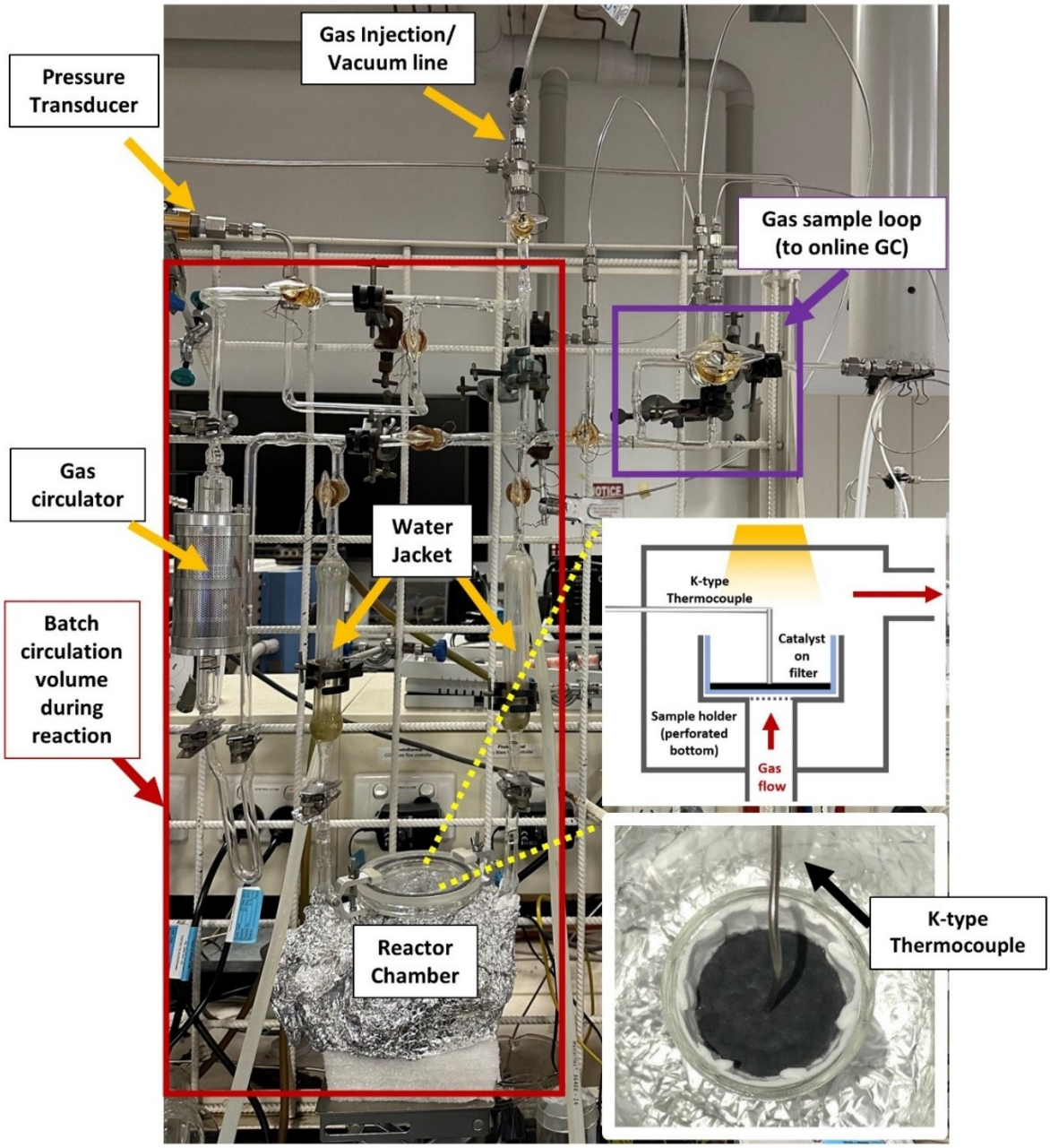

Figure S2.Photothermal (batch) reactor set-up.

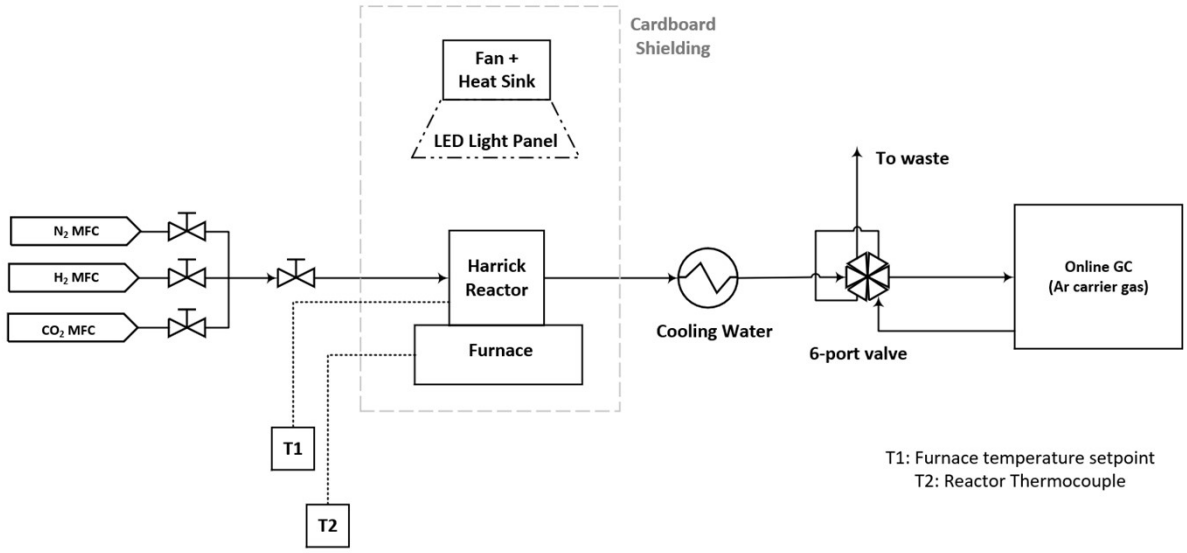

Figure S3. Schematic of flow mode Harrick reactor system used for CO_2 methanation reaction where reaction could be run with thermal heating under either dark or illuminated conditions.

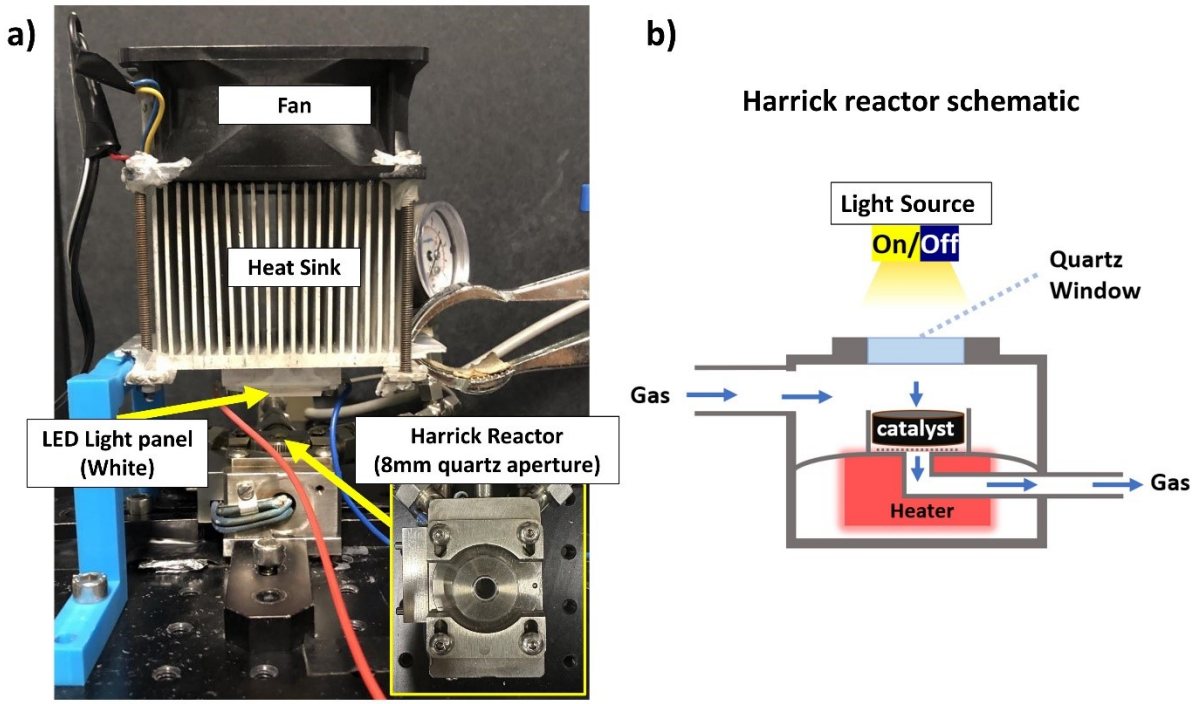

Figure S4. a) Harrick reactor set-up for visible light assisted thermal activity tests; b) schematic of the Harrick reactor used

Table S1. Ni loading (wt.%) on xNi-TiN samples obtained via ICP-OES

Sample	Nominal Ni loading (wt.%)	Actual Ni loading [a] wt.%
0.1Ni-TiN	10	10.1
0.4Ni-TiN	40	36.4
0.7Ni-TiN	70	65.4

[a]metallic Ni loading calculated based on Ni wt% (as NiO in as prepared samples) obtained from ICP-OES.

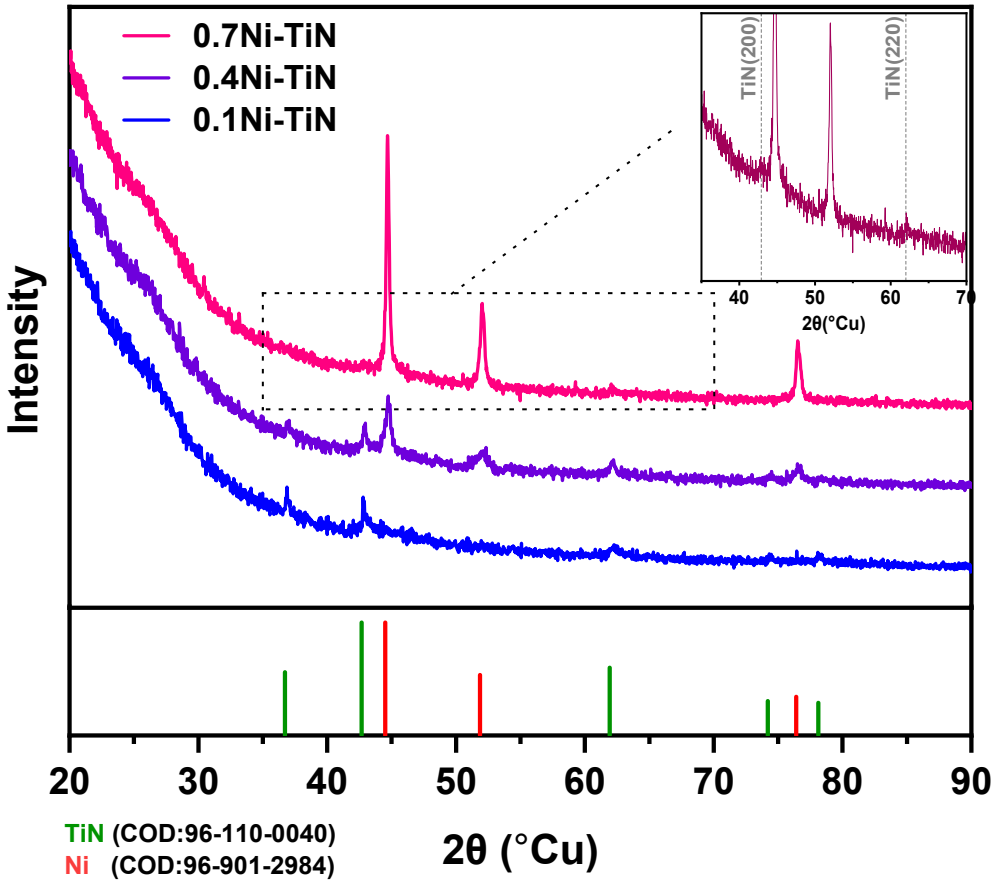

Figure S5. XRD spectra for reduced 0.1Ni-TiN, 0.4Ni-TiN, and 0.7Ni-TiN prior to preparation for TEM.

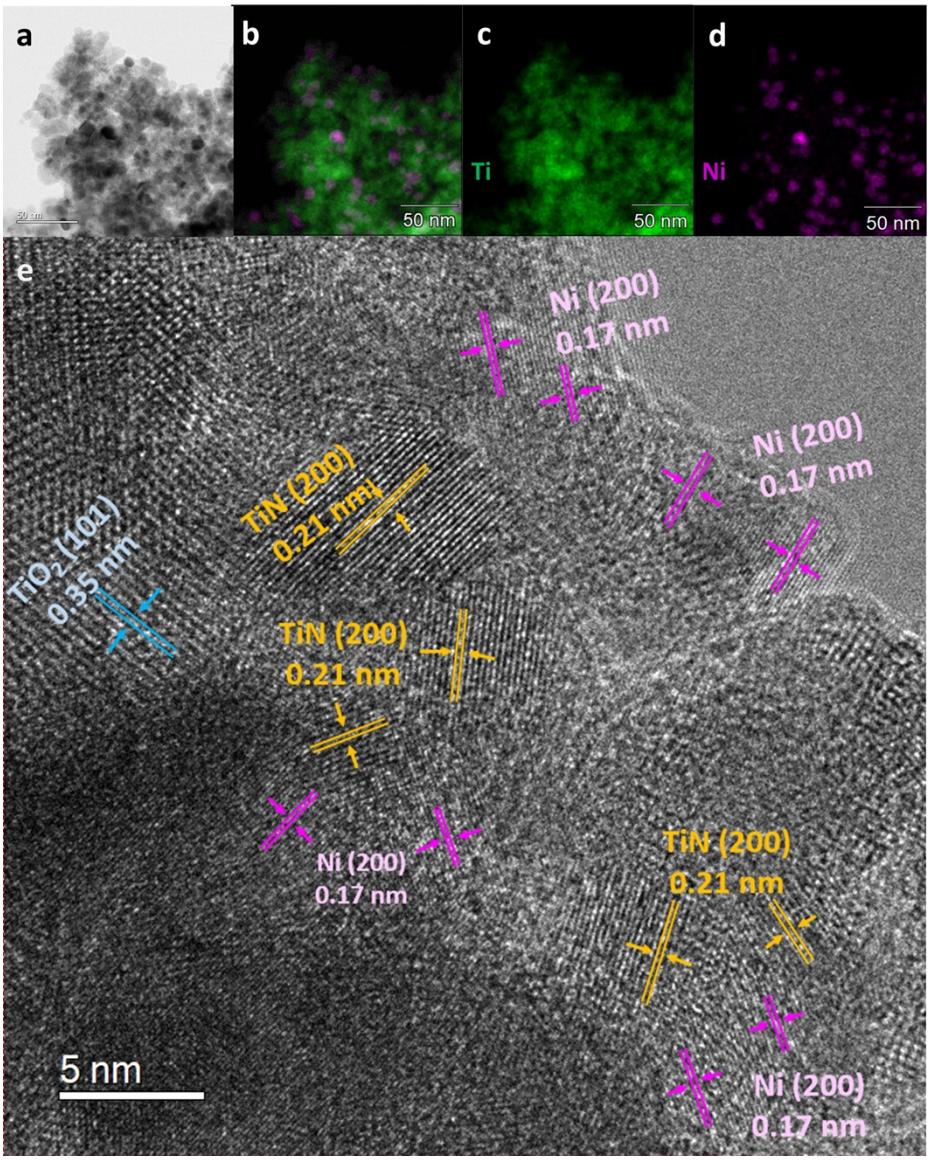

Figure S6. a) TEM micrograph of reduced 0.1Ni-TiN (r0.1Ni-TiN); b)-d) corresponding EDS mapping showing distribution of Ti (green) and Ni (magenta) content; e) HR-TEM micrograph of r0.1Ni-TiN demonstrating TiN(200) and Ni(200) lattice fringes.

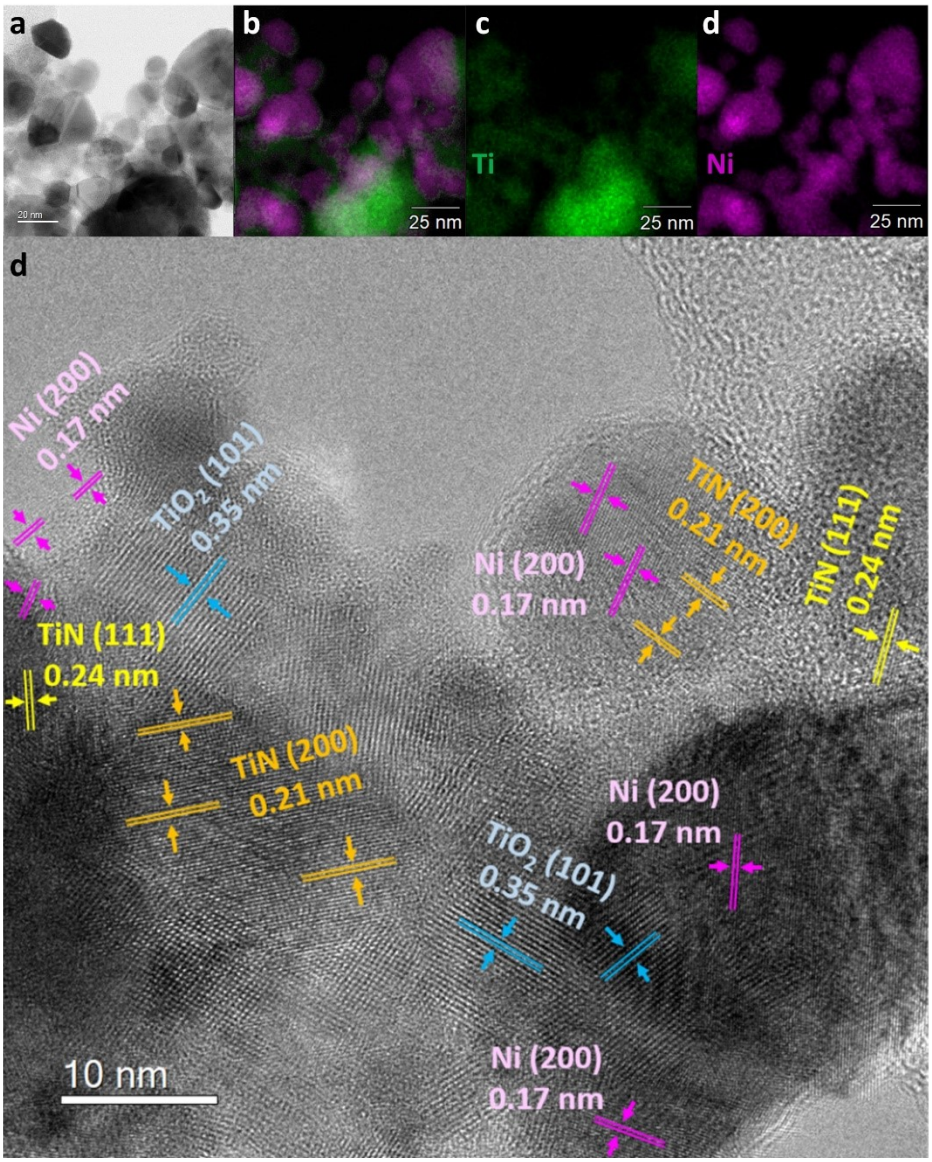

Figure S7. a) TEM micrograph of reduced 0.4Ni-TiN (r0.4Ni-TiN); b)-d) corresponding EDS mapping showing distribution of Ti (green) and Ni (magenta) content; e) HR-TEM micrograph of r0.4Ni-TiN demonstrating TiN(200), TiN(111) and Ni(200) lattice fringes.

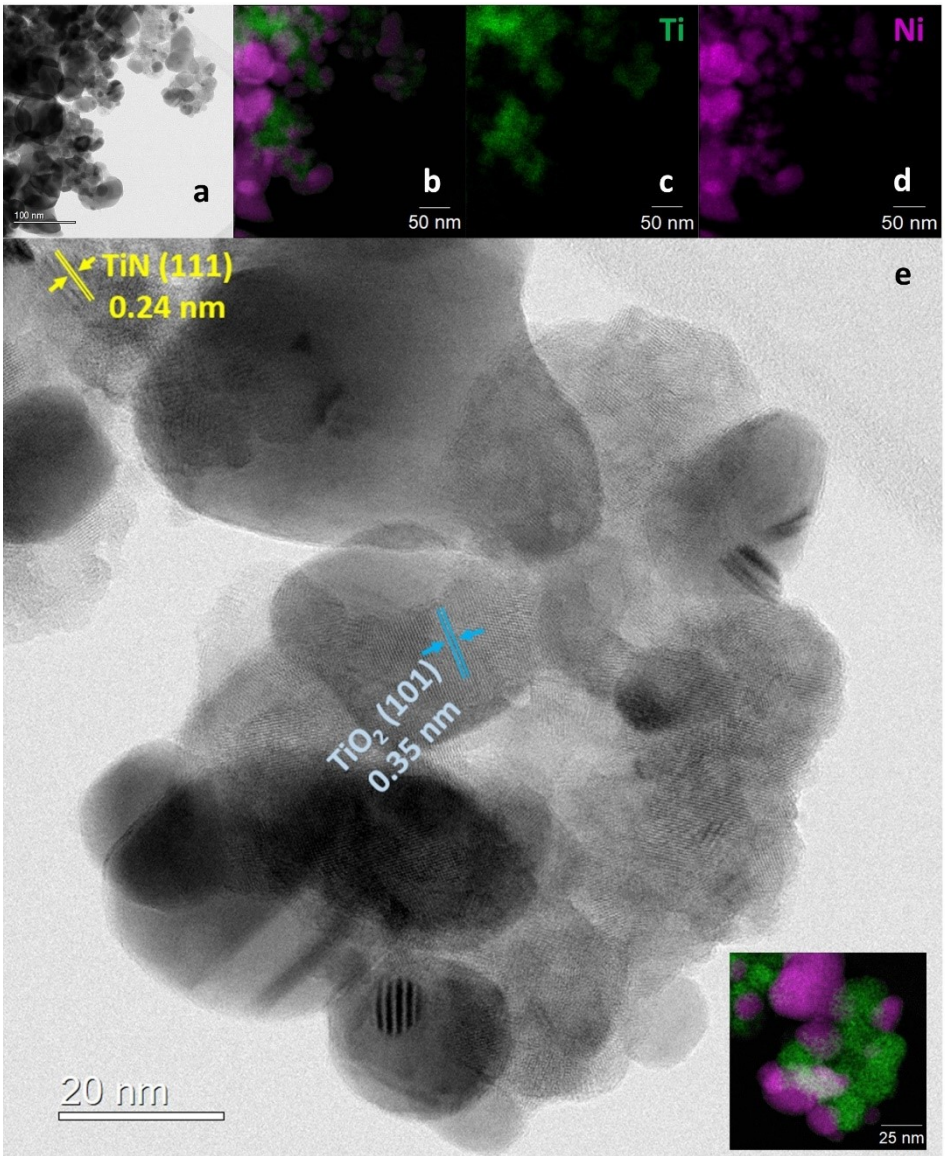

Figure S8. a) TEM micrograph of reduced 0.7Ni-TiN (r0.7Ni-TiN); b)-d) corresponding EDS mapping showing distribution of Ti (green) and Ni (magenta) content; e) TEM micrograph of r0.7Ni-TiN demonstrating TiN(111) and TiO_2(101) lattice fringes. EDS mapping Inset illustrates the location of metallic Ni. The Ni mapping does not overlap with O signal content.

On reducing the as-prepared xNi-TiN samples (rxNi-TiN), metallic Ni deposits are formed. For r0.1Ni-TiN (Figure S6) and r0.4Ni-TiN (Figure S7) lattice fringes for TiN (200) (d = 0.21nm), Ni(200) (d= 0.17nm) can be identified.[1-3] The TEM micrograph of r0.7Ni-TiN (Figure S8) indicates lattice fringes for TiN (111) (d = 0.24nm)[1] as well as large Ni particles, which is supported by corresponding EDS mapping. All three samples contain lattice fringes for TiO_2 (101) (0.35nm),[2] which is only observed in the bulk via TEM results. The TiO_2 presence derives from support oxidation during ex-situ sample preparation for microscopy. The reduced rxNi-TiN samples were first dispersed in methanol via ~20-minute sonication, then drop-cast onto a Cu-lacey carbon grid and dried in air. To validate

the TiN presence in the freshly reduced sample, XRD spectra of rxNi-TiN samples sealed in Kapton tape were recorded. The XRD spectra (Figure S5) confirm the presence of metallic Ni and cubic TiN. Additionally, XRD spectra of the as-prepared powder samples and spent samples, post-photothermal reaction (Figure S11), indicate no detectable catalyst oxidation before or during CO_2 methanation. The results illustrate the distinct difference in the Ni deposit morphology. A positive correlation between Ni loading and Ni deposit size after reduction and during methanation exists. The 0.1Ni-TiN contains small Ni deposits, while the 0.4Ni-TiN and 0.7Ni-TiN possess large metallic Ni deposits resulting in Ni-rich surfaces, particularly in the case of 0.7Ni-TiN which contains Ni particles independent of the support.

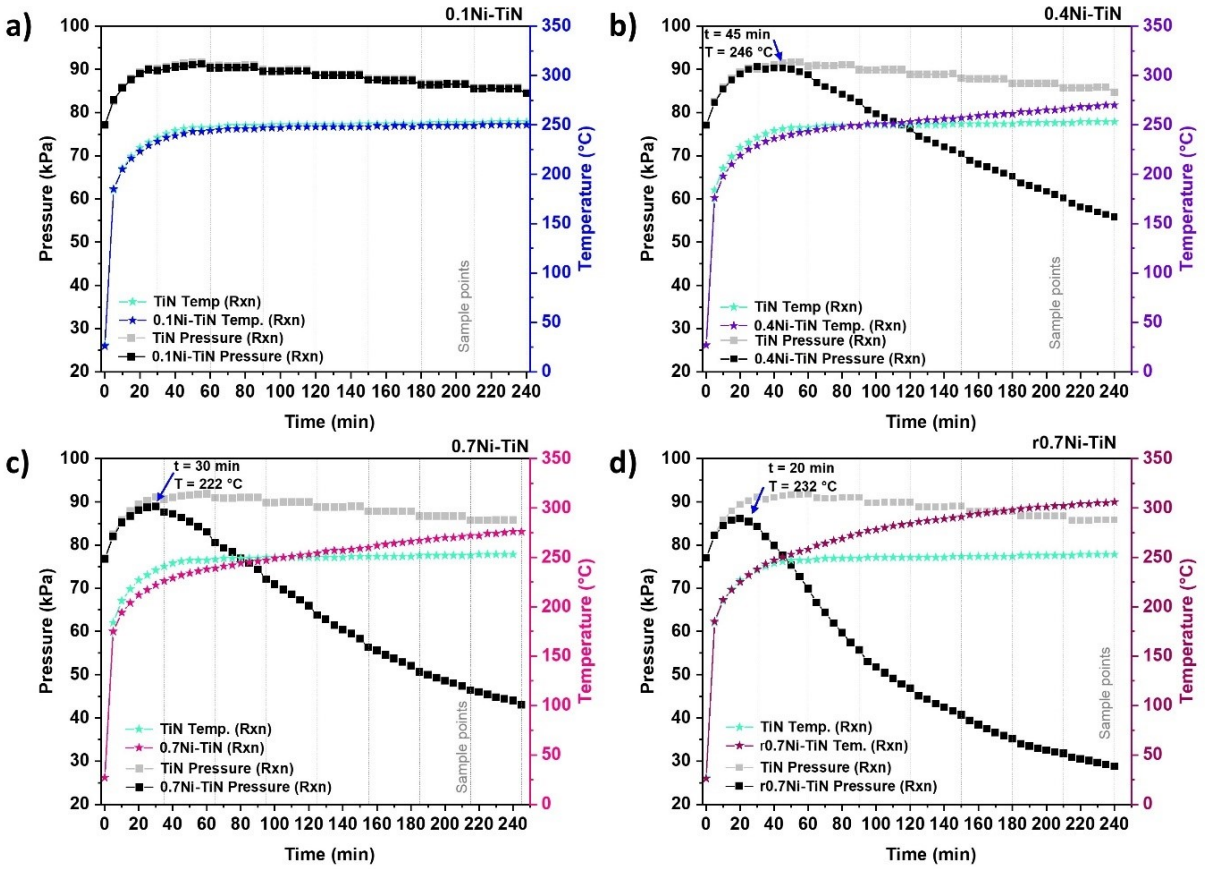

Figure S9. Reactor temperature and pressure profiles with time under photothermal reaction environment (batch system, ~79kPa starting pressure: 15kPa CO_2, ~60kPa H_2) for a) 0.1Ni-TiN; b) 0.4Ni-TiN; c) 0.7Ni-TiN; d) r0.7Ni-TiN. Blue arrow indicates the first sign of pressure decrease as a marker for reaction commencement.

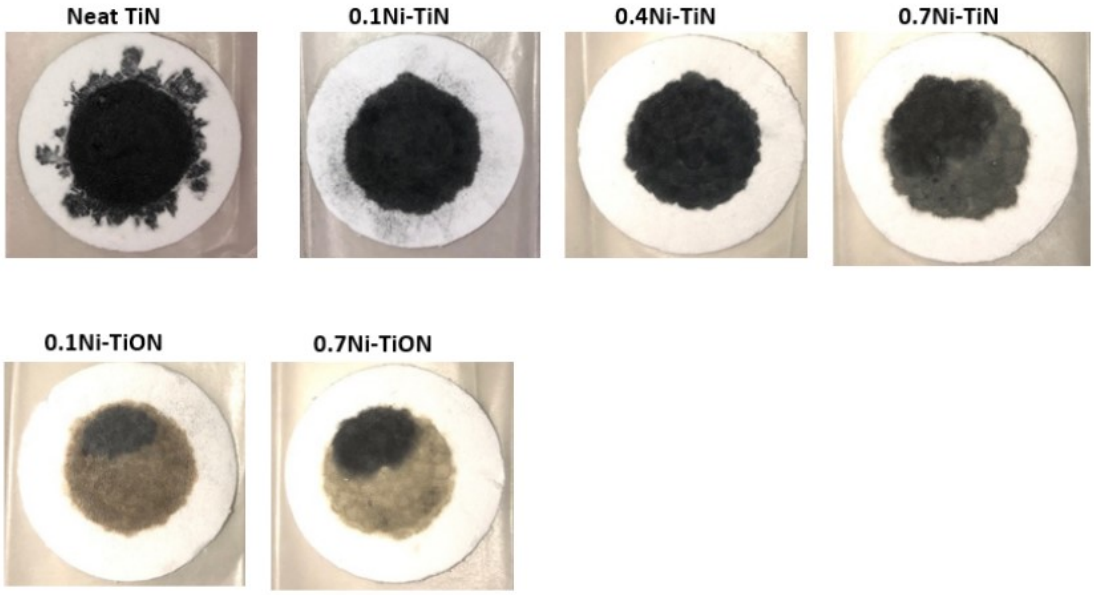

Figure S10. Spent catalyst samples from reaction under photothermal conditions in batch reactor. Xe lamp placement was fixed for all experiments. Discolouration (as-prepared samples colour changing from grey/brown to black) occurred where exposure to Xe lamp irradiation was the strongest, indicative of NiO reduction.

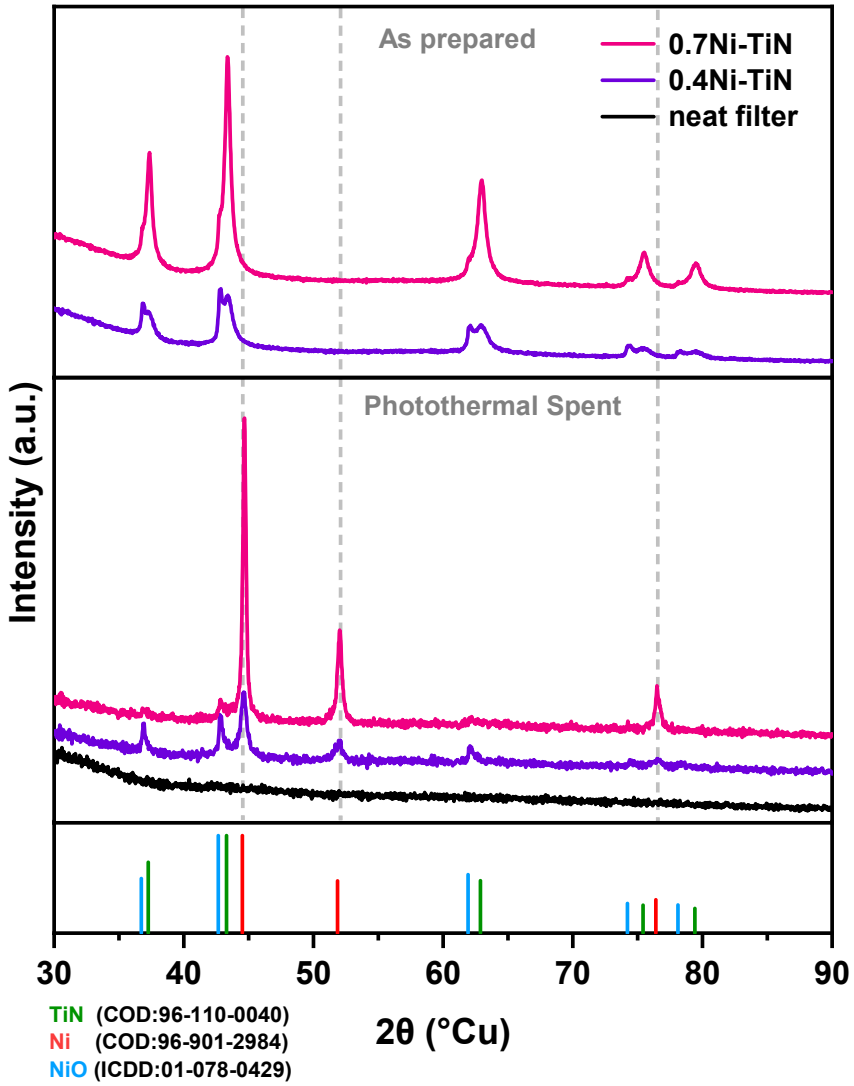

Figure S11. XRD spectra of as-prepared and spent (under photothermal conditions) 0.4Ni-TiN and 0.7Ni-TiN samples. The evolution of metallic Ni peaks (marked in grey) from NiO indicates sample reduction under photothermal conditions.

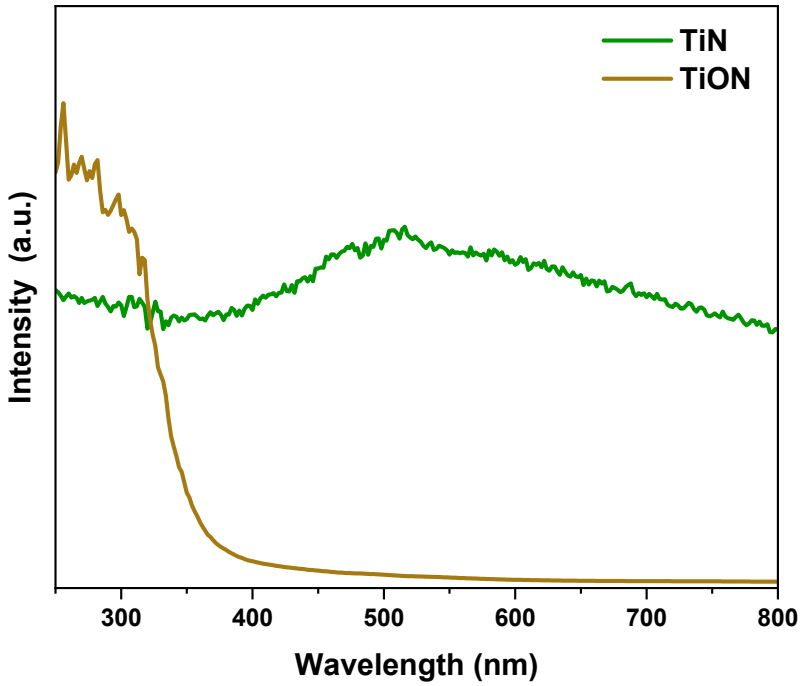

Figure S12. Comparison of UV-vis absorption by TiN and TiON. Oxidation of the TiN to TiON greatly reduces absorption by the support in the vis-NIR light region.

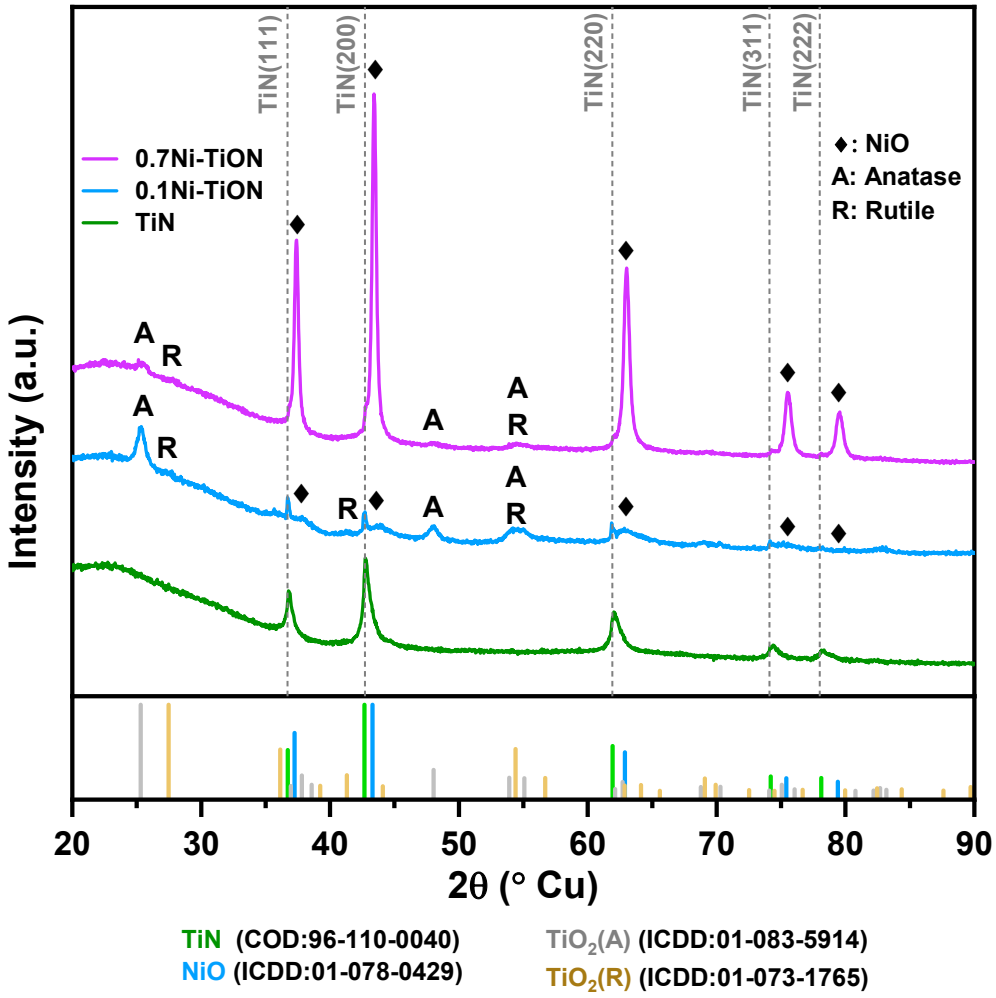

Figure S13. XRD spectra of neat TiN, 0.1Ni-TiON and 0.7Ni-TiON demonstrating the evolution of anatase and rutile phases due to support oxidation. The intensity of the NiO peak is seen to increase with Ni loading due to an increase in the sample content and crystallite size of NiO (A: anatase, R: rutile, ♦: NiO).

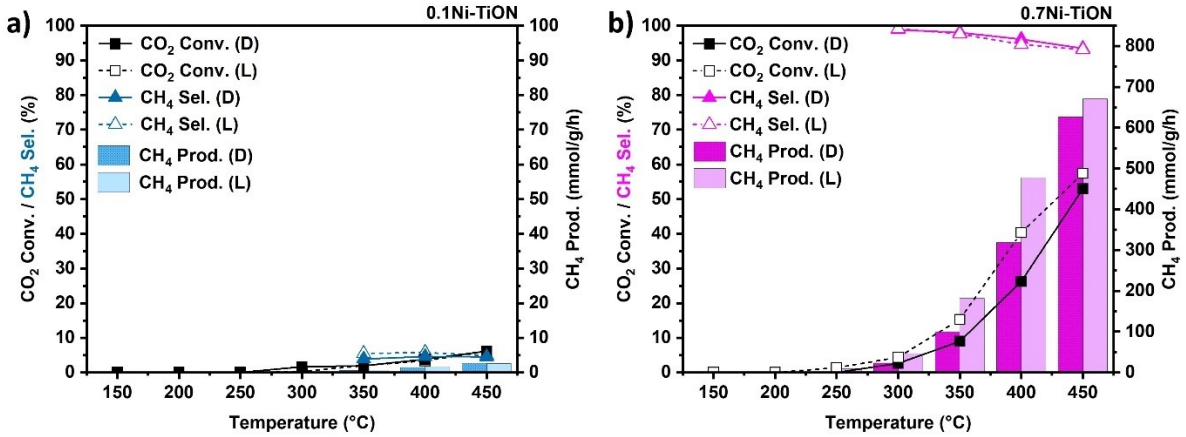

Figure S14. CO_2 conversion (Conv.), CH_4 selectivity (Sel.) and production (Prod.) with temperature for a) 0.1Ni-TiON and b) 0.7Ni-TiON under continuous flow mode conducted in dark (i.e., non-illuminated) and illuminated conditions at 150-450°C.

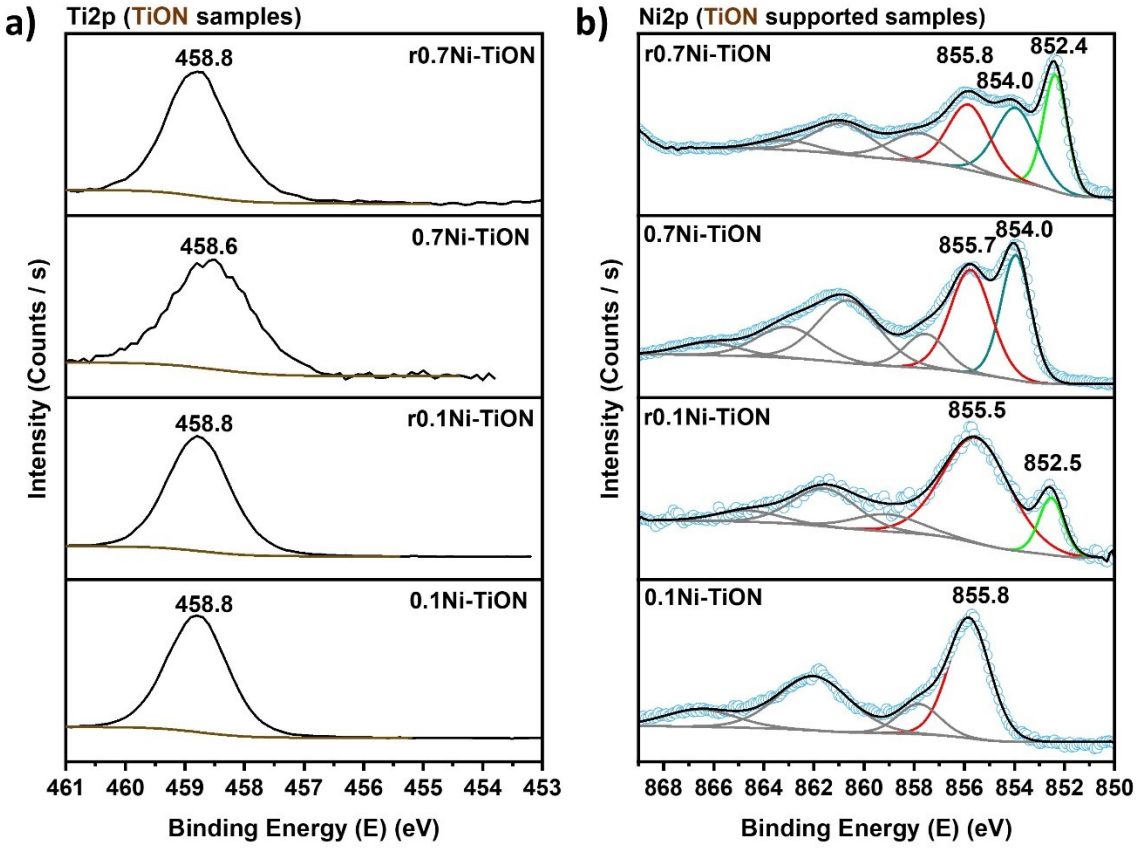

Figure S15. XPS spectra of the 0.1Ni-TiON and 0.7Ni-TiON samples across the a) Ti2p and b) Ni2p regions. Spectra are provided for both the as-prepared and pre-reduced (r) cases.

XPS spectra of the as-prepared and pre-reduced samples illustrate the dominant presence of Ti in the form of titania. TiN content appears to be preserved in the bulk of the samples given the presence of TiN-related peaks. Pre-reduction of the oxidised samples leads to the generation of metallic Ni species, which is evident in the evolution of the peak at ~852.5eV for both r0.1Ni-TiON and r0.7Ni-TiON.[4]

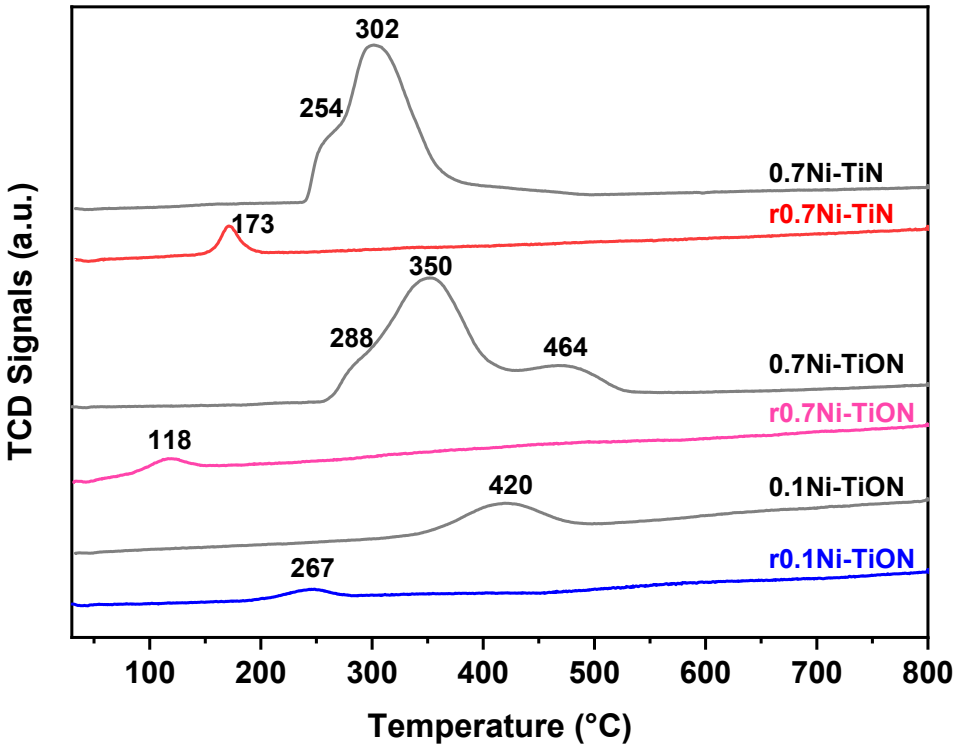

Figure S16. H_2-TPR profiles of 0.1Ni-TiON, 0.7Ni-TiON, and 0.7Ni-TiN, prior to and after pre-reduction (r).

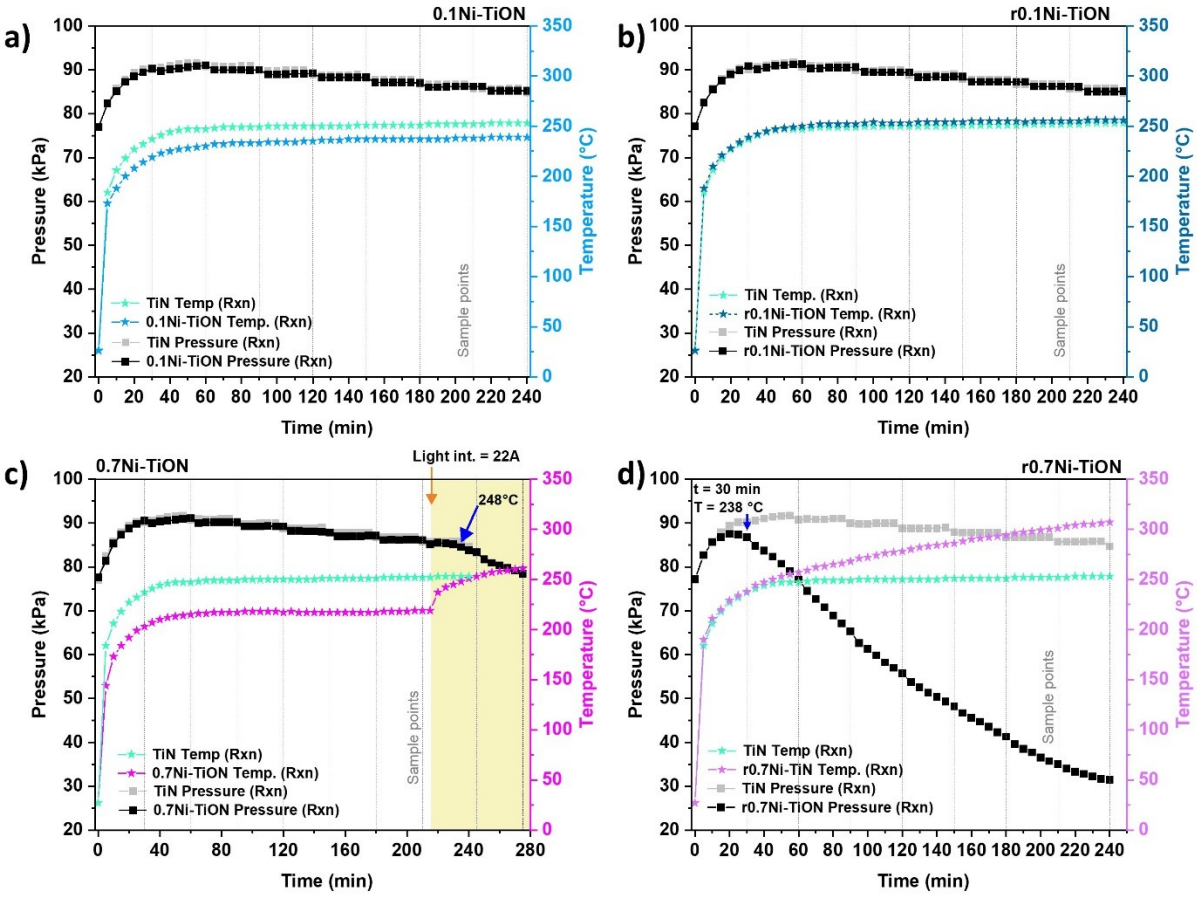

Figure S17. Reactor pressure and catalyst bed temperature profiles with time under photothermal reaction environment (batch system, ~79kPa starting pressure: 15kPa CO_2, ~60kPa H_2) for a) as-prepared and b) pre-reduced r0.1Ni-TiON and c) as-prepared and d) pre-reduced r0.7Ni-TiON. Profiles are plotted against conditions offered by neat TiN as a reference.

The as-prepared 0.1Ni-TiON and 0.7Ni-TiON samples are not active under the nominal 20A illumination. For 0.7Ni-TiON, the Xe lamp intensity was increased from 20A to 22A (maximum setting) at ~3.5h of illumination (Figure 9c), which saw the reaction commence when temperature reached 248°C.

Pre-reducing 0.1Ni-TiN (r0.1Ni-TiON) did not invoke catalytic activity for CO_2 methanation (Figure S17b). Pre-reducing the 0.7Ni-TiON (r0.7Ni-TiON) resulted in methanation under photothermal conditions (Figure S17d), evident by the significant decrease in reactor pressure along with a continuous increase in reactor temperature due to the onset of Ni reduction, and the ensuing reactant consumption and reaction exothermicity through CO_2 methanation. While the exposed TiON surface can be expected to be influenced by the presence of titania, a dependence on Ni availability for reaction is likely primarily responsible for catalyst activity.

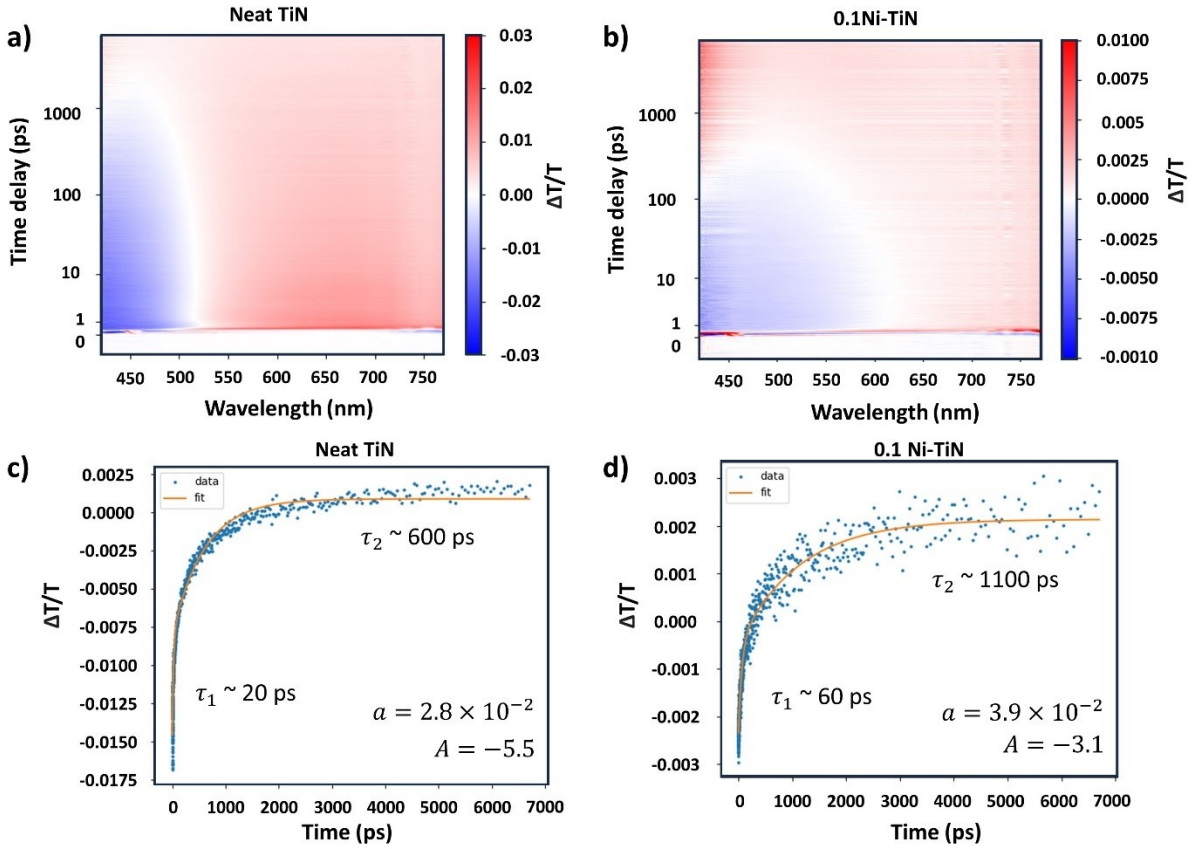

Figure S18. TA spectral maps of neat a) TiN and b) 0.1Ni-TiN; Kinetics decay fit at 450 nm probe for neat c) TiN, d) 0.1Ni-TiN, fit to the function $\frac{\Delta T}{T} = A\left[a\exp\left(-\frac{t}{\tau_1}\right) + (1-a)\exp\left(-\frac{t}{\tau_2}\right)\right]$. *Note the initial <500 fs time dynamics are not included in the kinetic fit as they arise from the solvent (glycerol) response.*

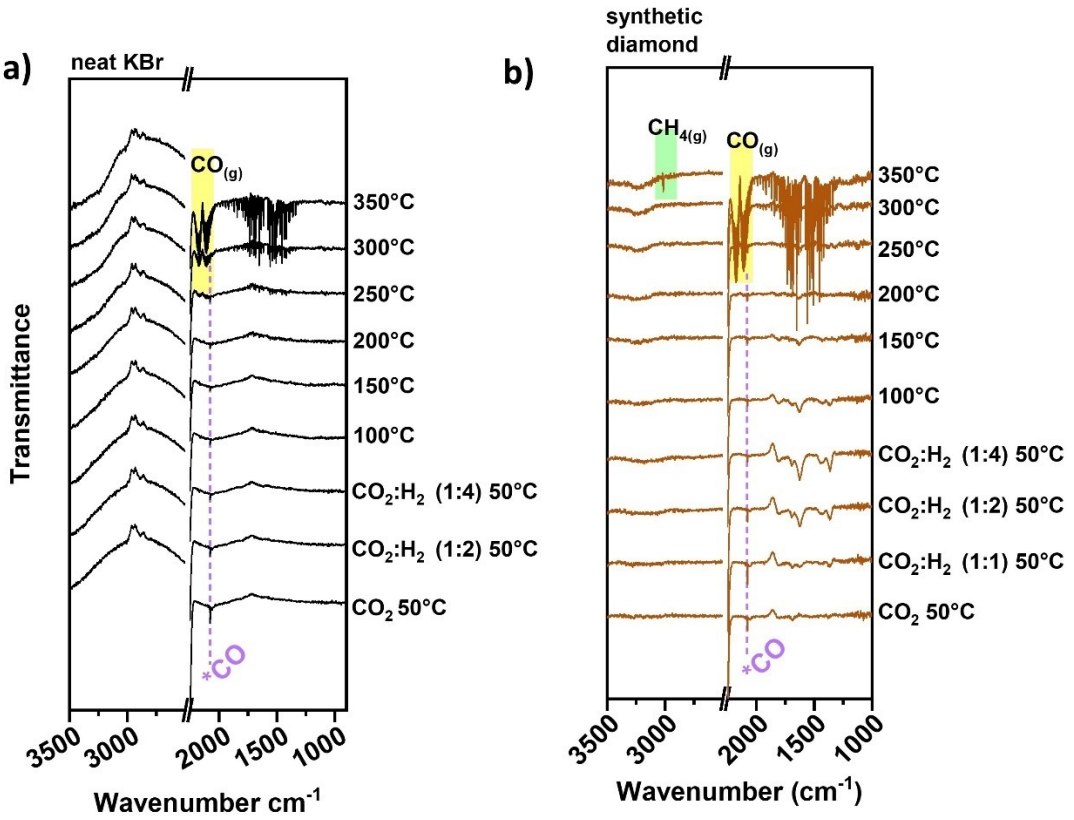

Figure S19. In-situ DRIFTS spectra under various conditions for a) calcined KBr and b) synthetic diamond

To determine whether there was any influence of the diluent used during in-situ DRIFTS analyses, the spectra of KBr and neat diamond under various reaction conditions were determined for reference. Figure S19a indicates that a small amount of *CO may be produced over the KBr surface under reaction conditions. In-situ DRIFTS spectra for synthetic diamond (Figure S19b) show the presence of intermediate peaks upon CO_2 introduction that are then consumed with the increase in temperature and hydrogen introduction. Figure 4c of the manuscript did not show signs of intermediate peaks over synthetic diamond-diluted TiN upon CO_2 introduction. This result suggests that TiN without significant CO_2 adsorption had diminished the negligible activity of synthetic diamond diluent. Additionally, for the TiN, 0.1Ni-TiN and 0.7Ni-TiN samples analysed by in-situ DRIFTS contributions from synthetic diamond/KBr cannot be completely excluded in formation of the observed *CO peak at 2076cm^{-1}.

*Table S2. Calculated adsorption energy of *CO_x over neutral Ni (111) and Ni cluster/TiN models.*

System	***CO_2 (Neutral)**	***CO (Neutral)**
Ni (111)	0.53 eV	-1.38 eV
Ni in **Ni cluster/TiN**	-0.18 eV	-1.13 eV

Table S3. Bader charge analysis over neutral and charged Ni (111) and Ni cluster/TiN models.

System	**-1 (Negative)**	**0 (Neutral)**	**+1 (Positive)**
Ni first layer in **Ni (111)**	-0.050	-0.019	0.004
Topmost Ni atom in **Ni cluster/TiN**	-0.217	-0.147	-0.07
TiN in **Ni cluster/TiN**	-0.560	0.253	1.075

Table S4. Calculated adsorption energy of *CO over neutral and charged Ni (111) and Ni cluster/TiN models.

System	**-1 (Negative)**	**0 (Neutral)**	**+1 (Positive)**
Ni (111)	-1.35 eV	-1.38 eV	-1.46 eV
Ni in **Ni cluster/TiN**	-1.30 eV	-1.13 eV	-1.01 eV

References

1. J. E. Oghenevweta, D. Wexler and A. Calka, *Journal of Materials Science*, 2018, **53**, 3064-3077.
2. T.-L. Thi Le, L. T. Nguyen, H.-H. Nguyen, N. V. Nghia, N. M. Vuong, H. N. Hieu, N. V. Thang, V. T. Le, V. H. Nguyen, P.-C. Lin, A. Yadav, I. Madarevic, E. Janssens, H. V. Bui and L. L. Ngoc, *Journal*, 2021, **11**.
3. Q. Zhou, Q. Hao, Y. Li, J. Yu, C. Xu, H. Liu and S. Yan, *Nano Energy*, 2021, **89**, 106402.
4. S. H. Gage, C. Ngo, V. Molinari, M. Causà, R. M. Richards, F. S. Gentile, S. Pylypenko and D. Esposito, *J. Phys. Chem. C*, 2018, **122**, 339-348.